Carbon Trends 12 (2023) 100282

Contents lists available at ScienceDirect

Carbon Trends

journal homepage: www.elsevier.com/locate/cartre

Antimicrobial graphene-based coatings for biomedical implant applications

Jesus Romo-Rico[a,b], Richard Bright[c], Smriti Murali Krishna[b,d], Krasimir Vasilev[c], Jonathan Golledge[b,e], Mohan V. Jacob[a,*]

[a] Electronics Materials Lab, College of Science and Engineering, James Cook University, Townsville, QLD 4811, Australia
[b] Queensland Research Centre for Peripheral Vascular Disease, James Cook University, Australia
[c] College of Medicine and Public Health, Flinders University, Bedford Park, South Australia, Australia
[d] Atherothrombosis and Vascular Biology, Baker Heart and Diabetes Institute, Melbourne 3004, Australia
[e] Department of Vascular and Endovascular Surgery, Townsville University Hospital, Townsville, QLD 4811, Australia

ARTICLE INFO

Keywords:
Antimicrobial
Biocompatible
Graphene
Coatings
Implant

ABSTRACT

Implant-associated infections (IAI) cause significant health issues and healthcare costs. In this research, we deposited graphene (Gr) on a medical-grade cobalt-chromium (CoCr) alloy surface by radiofrequency plasma-enhanced chemical vapor deposition (RF-PECVD) using *Origanum vulgare* as a precursor material. The deposition of Gr on the CoCr was confirmed using Raman spectroscopy and X-Ray photoelectron spectroscopy (XPS) and scanning electron microscopy (SEM). The biocompatibility and antibacterial properties of CoCr-Gr were investigated. CoCr-Gr was biocompatible and promoted cell adhesion and spreading of RAW 267.4 macrophage cells. CoCr-Gr were antibacterial against *Staphylococcus aureus* and *Pseudomonas aeruginosa* and inhibited *P. aeruginosa* attachment. The results indicate that CoCr-Gr could be used as a potential antibacterial coating material for implantable devices.

1. Introduction

Implant-associated infection (IAI) is a major global burden associated with morbidity, mortality and high healthcare cost [1,2]. The incidence of IAI with some devices can be as high as 30% [3]. The total cost of treating IAI varies depending on the primary treatment option chosen, with debridement, antibiotics and implant retention (DAIR) resulting in the lowest cost at A$19,688, followed by excision arthroplasty at A$23,805, one-stage revision at A$26,722, and two-stage revision at A$44,744, according to a study of 114 patients who underwent a total of 178 surgical procedures for IAI treatments in Australia [4]. IAI occurs when bacteria enter the body through the implant site, attach to the device and start to form a biofilm [5]. The antibiotic resistance of a biofilm is significantly stronger than in planktonic cells and the infection becomes difficult to eradicate [6,7]. The number of infections caused by antibiotic-resistant is constantly increasing, and this trend is projected to continue [8]. Therefore, the demand for developing novel coatings with enhanced properties to reduce the risk of IAI is very high [9].

Graphene-based coatings have been used in wound healing applications [10,11]. Studies have shown that graphene coatings can inhibit the growth of a wide range of bacteria [12,13]. Typically, graphene oxide (GO) sheets were deposited by electrophoretic deposition on plasma electrolytic oxidation (PEO) pre-treated titanium (Ti) substrates. The GO enhanced the antibacterial activity of the PEO-Ti samples by reducing ~80% and ~100% of *Escherichia coli* and *S. aureus* viability, respectively [14]. In other studies, spark plasma sintering (SPS) was used to incorporate graphene into a magnesium alloy implant, which reduced *S. aureus* and *E. coli* viability up to 5-fold. The cytocompatibility with human mesenchymal stromal cells (hMSCs and osteogenic properties were also enhanced by graphene-modified surfaces [15].

Cobalt-chromium (CoCr) alloys are commonly used for orthopedic, dental, and cardiovascular implants [16,17]. Despite its excellent mechanical properties, wear resistance and biocompatibility, like other metal alloys, CoCr alloys have their drawbacks [18,19]. CoCr alloys are susceptible to bacterial infection due to contamination introduced by poor sterilization and on-sterile/handling, causing inflammation, allergic reaction and aseptic loosening [20]. Graphene has been incorporated into CoCr alloys in an attempt to enhance their properties [21]. For example, GO was electrodeposited onto medical cobalt-chromium-molybdenum (CoCrMo) alloys and coated with ε-poly-L-Lysine (ε-PLL) to endow it with antibacterial properties. The integration of GO, as well as ε-PLL and GO/ε-PLL on CoCrMo alloys, increased antibacterial activity against *S. aureus* and *E. coli* [22].

* Corresponding author.
E-mail address: mohan.jacob@jcu.edu.au (M.V. Jacob).

https://doi.org/10.1016/j.cartre.2023.100282
Received 3 April 2023; Received in revised form 3 July 2023; Accepted 3 July 2023

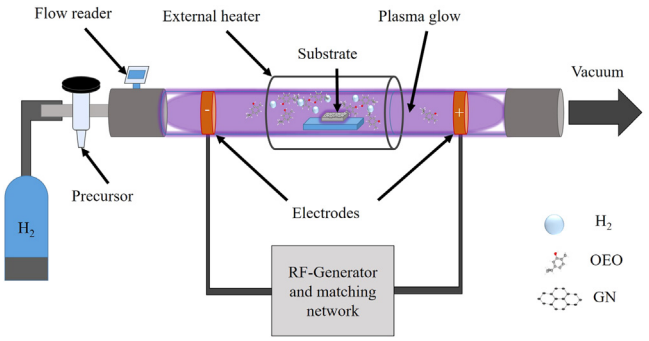

Fig. 1. Representation scheme of the RF-PECVD system utilized to fabricate Gr on CoCr substrate.

Radiofrequency plasma-enhanced chemical vapor deposition (RF-PECVD) has been used to fabricate graphene from renewable precursors, such as plant secondary metabolites for their use in electronics applications such as sensors and organic photovoltaic cells [23]. RF-PECVD graphene derived from Pelargonium graveolens was directly deposited on silicon oxide and quartz substrates by Al-Jumaili et al. The plasma-induced fabrication of vertically oriented graphene nanowalls which were functioning as graphene knives damaged *E. coli* and *S. aureus* membranes [24].

This study aims to fabricate a graphene coating on the CoCr alloy surface by RF-PECVD using *Origanum vulgare* as a precursor material. To the best of our knowledge, the incorporation of graphene coatings into CoCr alloy surfaces by RF-PECVD using *Origanum vulgare* as a graphene precursor has not been studied yet. *Origanum vulgare* essential oil is primarily composed of volatile organic compounds such as monoterpenes and sesquiterpenes, containing a high amount of carbon that can potentially serve as a graphene precursor. Therefore, this plant was selected as a suitable source for the fabrication of graphene.

The surface was characterized by Raman, Wettability, X-ray photoelectron spectroscopy (XPS) and scanning electron microscopy (SEM). The biocompatibility of the graphene coating with mammalian cells was investigated. We also evaluated the antibacterial properties of the graphene coating against Gram-positive and Gram-negative bacteria.

2. Experimental

2.1. Materials

Medical grade CoCr alloy (L605, ASTM F90, $Ø_{ext}$ = 2.5 mm, $Ø_{int}$ = 2.28 mm) was received as a sample from Minitubes® (Grenoble, France). *Origanum vulgare* was purchased from Sydney Essential Oils Company (Sydney, Australia).

2.2. Synthesis of Gr on CoCr substrates

Graphene was directly deposited by RF-PECVD on CoCr substrates. Before the fabrication, the CoCr tube was flattened and cut using a diamond disk in rectangle substrates (3 × 7 mm). CoCr substrates were sonicated and cleaned with isopropyl alcohol for 5 min and air-dried before placing them in the middle of the plasma reactor.

The custom RF-PECVD reactor is represented in Fig. 1; it is composed of a quartz tube covered with a ceramic furnace coupled with an external heater [24,25]. On one end of the plasma reactor, an H_2 delivery system, a flask, a stopcock, and a flow meter are connected. On the other end, the quartz tube is connected to a vacuum pump. Before the Gr fabrication, the CoCr substrate were pre-treated with H_2 and plasma power of 500 W at 10 sccm, and 700 °C for 1 min. A rotary pump was utilized to maintain the plasma reactor at 0.02 mbar. *Origanum vulgare* vapours were then introduced into the plasma reactor using the manual stopcock flow controller meanwhile the plasma discharge was kept for 4 min.

2.3. Raman and X-ray photoelectron spectroscopy

Raman spectroscopy was used to characterize the CoCr-Gr at room temperature with a WITec's Raman Spectrometer (WITec, Ulm, Germany). The laser wavelength utilized was, λ = 532 nm. X-ray photoelectron spectroscopy (XPS) was carried out using a Kratos AXIS Ultra DLD spectrometer (Kratos Analytical Ltd., Manchester, UK), which uses a monochromatic AlKα radiation (hν = 1486.7 eV). Data were analyzed with CasaXPS software (Casa Software Ltd., Teignmouth, UK).

2.4. Contact angle

The water contact angle (WCA) of CoCr and CoCr-Gr was determined using a sessile drop method with a KSV CAM 101 optical apparatus (KSV Instruments Ltd., Helsinki, Finland). The contact angle of an 8 μl drop of MiliQ water was measured using the CoCr and CoCr-Gr surfaces of the samples as a baseline reference.

2.5. Scanning electron microscopy

CoCr and CoCr-Gr surfaces were imaged using a Zeiss Merlin FEG-SEM, (Microscopy Australia, University of South Australia: Zeiss, Jena, Germany). The images were taken using an accelerating voltage of 2 kV, and magnifications of 10 K and 20 K.

2.6. Raw 264.7 macrophage-like cells culture

Macrophages are one of the first immune cells to interact with an implant surface and play an essential role in innate immunity, bone remodeling and wound healing [26]. RAW 264.7 macrophage-like cells (Abelson leukemia virus-transformed cell line derived from BALB/c mice, ATCC TIB-71) were cultured in Dulbecco's modified Eagle's medium (DMEM; ThermoFisher, CA, USA) media was supplemented with 10% Fetal Bovine Serum (FBS, Life Technologies, CA, USA) plus 1% Pen/Strep (100 U/mL Penicillin and 100 μg/mL Streptomycin, Life Technologies, CA, USA) and incubated at 37 °C in 5% CO_2.

2.7. Cell viability (MTT assay)

Before the MTT (3-(4,5-Dimethylthiazol-2-yl)−2,5-diphenyltetrazolium bromide, Sigma-Aldrich, MI, USA) the assay was performed in a 24-well plate, CoCr and CoCr-Gr samples were placed into 24 well-plate and UV sterilized for 20 min. Macrophages were seeded on sample surfaces at a density of 2 × 10^5 cells/mL in 1 mL of RPMI supplemented with 10% Fetal Calf Serum (FCS) and 1% Pen/Strep v/v and incubated for 48 h. A working stock of MTT in PBS was prepared at 5 mg/ml, and 100 μl of MTT/PBS concentration was added into each well and then incubated for 4 h at 37 °C in 5% CO_2. Next, the solution was removed and 200 μl DMSO was added to each sample to lyse the cells. The well plate was stored in the dark for 15 min before reading its absorbance at 570 nm.

2.8. Cell adhesion and spreading

The cells were PBS-washed twice and permeabilized using 0.1% Triton X-100 diluted in 1x PBS for 5 min, then 1% BSA diluted in 1x PBS was added for 30 min. The two washing steps were repeated before TRITC-conjugated Phalloidin (FAK100 kit, Sigma-Aldrich) and PBS were added (1:1000 dilution) to the samples and incubated for 1 h. Phalloidin is a fluorescent dye used to stain actin filaments of cells, which are indicators of cell adhesion and spreading. Cell nuclei were stained incubating cells with DAPI for 5 min. Cells were washed thrice with PBS for 10 min. Then, CoCr and CoCr-Gr were mounted on microscope slides by using

an antifade mounting solution. Olympus FV3000 confocal microscope (CLSM; Olympus, Tokyo, Japan) was used to take fluorescence images of each sample.

2.9. Bacterial studies

Bacteria were recovered from glycerol stocks, *S. aureus* (ATCC 25923) and *P. aeruginosa* (clinical isolate, PAO1 type; SA Pathology) and plated on tryptone soy agar plate (TSA; Oxoid, Thermofisher, MA, USA) and incubated at 37 °C for 18 h. Next, single colonies of each pathogen were inoculated into tryptone soy broth (TSB, Oxoid, ThermoFisher, MA, USA) and 5% FCS (TSBFCS; Gibco, ThermoFisher, MA, USA) and incubated at 37 °C for 18 h. Cell density was adjusted to 1×10^9 CFU/mL by measuring the absorbance at 600 nm using a NanoDrop™ 2000c (ThermoFisher, MA, USA) and incubated at 37 °C for 18 h. Finally, bacterium cultures were diluted down to 1×10^6 CFU/mL and 1 mL of each dilution was added to CoCr and CoCr-Gr.

2.10. Scanning electron microscopy of bacterial morphology

To observe *S. aureus* and *P. aeruginosa* morphology, both pathogens were cultured on the CoCr and CoCr-Gr surfaces and images using a scanning electron microscope (SEM). After inoculating the samples with *S. aureus* or *P. aeruginosa* for 24 h, the culture media was removed from each sample and washed twice with PBS to remove loosely attached bacteria. The samples were then dehydrated using increasing concentrations of ethanol (50, 75 and 100% v/v), followed by a 1:1 mix of 100% ethanol and hexamethyldisilazane (HMDS, Sigma-Aldrich, MA, USA) for 20 min, and 100% HMDS for 20 min. The samples were left to dry for 3 h and mounted on aluminum stubs (using double side carbon tape) and sputter coated with 5 nm platinum. The same SEM voltage, magnification and working distance used in the surface morphology SEM were used in these experiments.

2.11. Live/dead bacteria assay

After the bacteria were incubated on CoCr and CoCr surfaces, a Live/Dead® BacLight™ kit (Invitrogen, ThermoFisher MA, USA) was utilized to observe and quantify the viability of the bacteria. The assay was performed according to the manufacturer's protocol. This assay uses Syto9, a green fluorescence dye that binds to live cell nucleic acids, and propidium iodide, a red fluorescence dye that stains damaged bacteria and dead cells. The samples were submerged in 1.5 μl of Syto9 (Ex/Em 480/500 nm) and 1.5 μl of Propidium Iodide (PI; Ex/Em 490/635 nm) per mL of PBS, for 15 min at RT in the dark. Thereafter, a confocal laser scanning microscope (Olympus FV3000) was used to take three random images of each sample (magnification x40). Cell viability and cell number were quantified using ImageJ software (V1.53t: NIH, MD, USA).

2.12. Statistical analyses

In the bacterial and cell viability experiments, a total of three biological replicates were conducted for each experiment. The mean and standard deviation of the replicates were plotted in GraphPad Prism (v8.3.0). To determine statistical significance, a two-way analysis of variance (ANOVA) with Sidak's multiple-comparisons test was performed using the aforementioned software.

3. Results and discussion

3.1. Surface characterization

Raman spectroscopy was used to analyze the plasma-fabricated CoCr-Gr. The Raman spectra in Fig. 2 A highlight the presence of intense D, G, and 2D peaks of sp2 carbon structure at 1341, 1569, and 2680 cm^{-1}, respectively. These peaks are typical of graphene with high content of defects [27]. The D-peak occurs at 1341 cm^{-1} due to the scattering of phonons produced by the defects on the disordered edge of the Brillouin zone. The G-peak, located at 1569 cm^{-1}, is associated with the vibrational modes of sp2-bonded carbon and the crystallinity of the graphene. The 2D peak at 2680 cm^{-1} occurs from two phonon vibration modes and is related to the number of graphene layers [28].

The ID/IG ratio is an indicator of the structural quality of graphene. A lower ID/IG ratio indicates a higher degree of crystallinity and a more ordered structure, while a higher ID/IG ratio suggests a higher concentration of defects and disorders in the graphene material. In this study, the ID/IG ratio for the CoCr-Gr samples is 0.72, which can be associated with a few layers of graphene [29].

The WCA results of CoCr and CoCr-Gr are presented in Fig. 2 B. CoCr and CoCr-Gr WCA were 58 ± 8.9 and 57 ± 3.8, respectively ($n = 3$). WCA measurements indicate that both surfaces were relatively hydrophilic [30,31]. Hydrophilic surfaces are considered to capacity to decrease immune reactions and accelerate implant integration [32,33].

Fig. 2 C and 2 D show the XPS survey and high-resolution C1s spectra of CoCr-Gr deposited with RF-PECVD. Survey spectra in C show a strong C1s-peak located at 284.4 eV, which can be associated with the sp^2 carbon hybridization (C=C) of graphitic carbon [34]. The sp^3 hybridization of carbon at 284.9 eV corresponds to aliphatic hydrocarbon groups (C—H and C—H–C), [34].

These groups can be related to edges and defects in the graphite nanostructures exposed to high temperatures, it is established that Gr tends to absorb atmospheric moisture [35,36]. A low-intensity peak related to the π-π^* energy loss is located at 286.7 eV [35]. The O1s peak is observed at the binding energy of 533 eV. A shoulder peak at 531.9 eV can be attributed to C=O interactions [37]. CoCr-associated peaks, Co2p and Co 2p1/2 are located at 779.35 and 793 eV, respectively. As well as for Cr21/2 is located at 586.5 eV and Cr2p at 576.8 eV.

The SEM micrographs in Fig. 2 E and 2 F show the CoCr and CoCr-Gr, respectively. The CoCr control surface shows the alloy microstructure containing grain boundaries, defects and agglomerations [38]. The SEM micrographs of CoCr-Gr corroborated the presence of Gr nanosheets on the CoCr-Gr surface [39]. The CoCr-Gr micrographs show Gr in the form of nanostructures with random shapes and sizes <100 nm. There are few Gr nanosheets >100 nm. These Gr formations can be associated with the high content of defects found in the chemical characterization.

3.2. Biocompatibility and focal adhesion of raw macrophages on CoCr-Gr

An MTT assay was used to determine cell viability based on the conversion of the yellow tetrazolium salt MTT to purple formazan by living cells at 48 h by measuring cellular metabolic activity on RAW macrophages incubated onto CoCr and CoCr-Gr surfaces. Both samples have shown similar cell viabilities without significant difference, as it's seen in the MTT plot shown in Fig. 3 A. Fig. 3 B shows the corrected total fluorescence calculated using ImageJ. The fluorescence images in Fig. 3 C show the morphology and the actin cytoskeleton of 264.7 RAW macrophages incubated with CoCr and CoCr-Gr after 48 h. F-actin (red staining) appeared well-defined and showed normal cell spreading. F-actin filaments provide mechanical stability to the cell cytoskeleton and the cell cortex in mammalian cells and play a role in cell migration and cell adhesion [40]. DAPI (blue staining) shows the nuclei of cells with healthy morphology. Overall, there were no differences between the cytotoxicity and adhesion of RAW macrophages incubated onto CoCr and CoCr-Gr for 48 h.

3.3. Bactericidal and antifouling effects of CoCr-Gr

The bactericidal and antifouling properties of the CoCr and CoCr-Gr were studied in cultures of *P. aeruginosa* and *S. aureus* as representative of Gram-negative and Gram-positive pathogens often causing medical device associated infections. After inoculation on the surface for 18 h

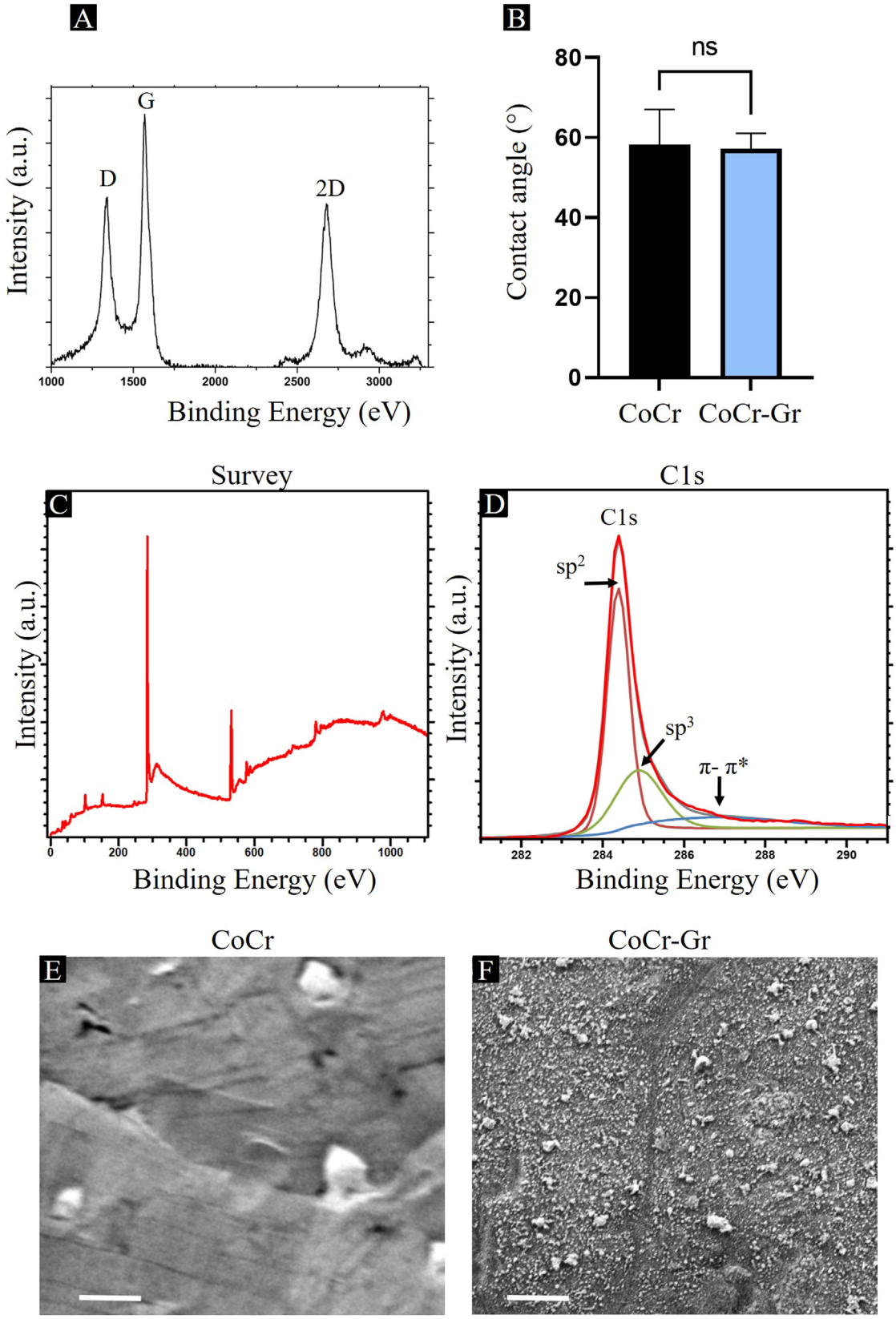

Fig. 2. A shows Raman spectra of CoCr-Gr, showing D, G and 2D peaks of graphene. The water contact angle of CoCr and CoCr-Gr is shown in 2 B. XPS of CoCr-Gr 2C shows normalized survey and 2 D displays high-resolution C1s spectra and hybridizations of carbon. 2 E and 2 F show SEM of CoCr and CoCr-Gr, respectively. Scale bar 1 μm.

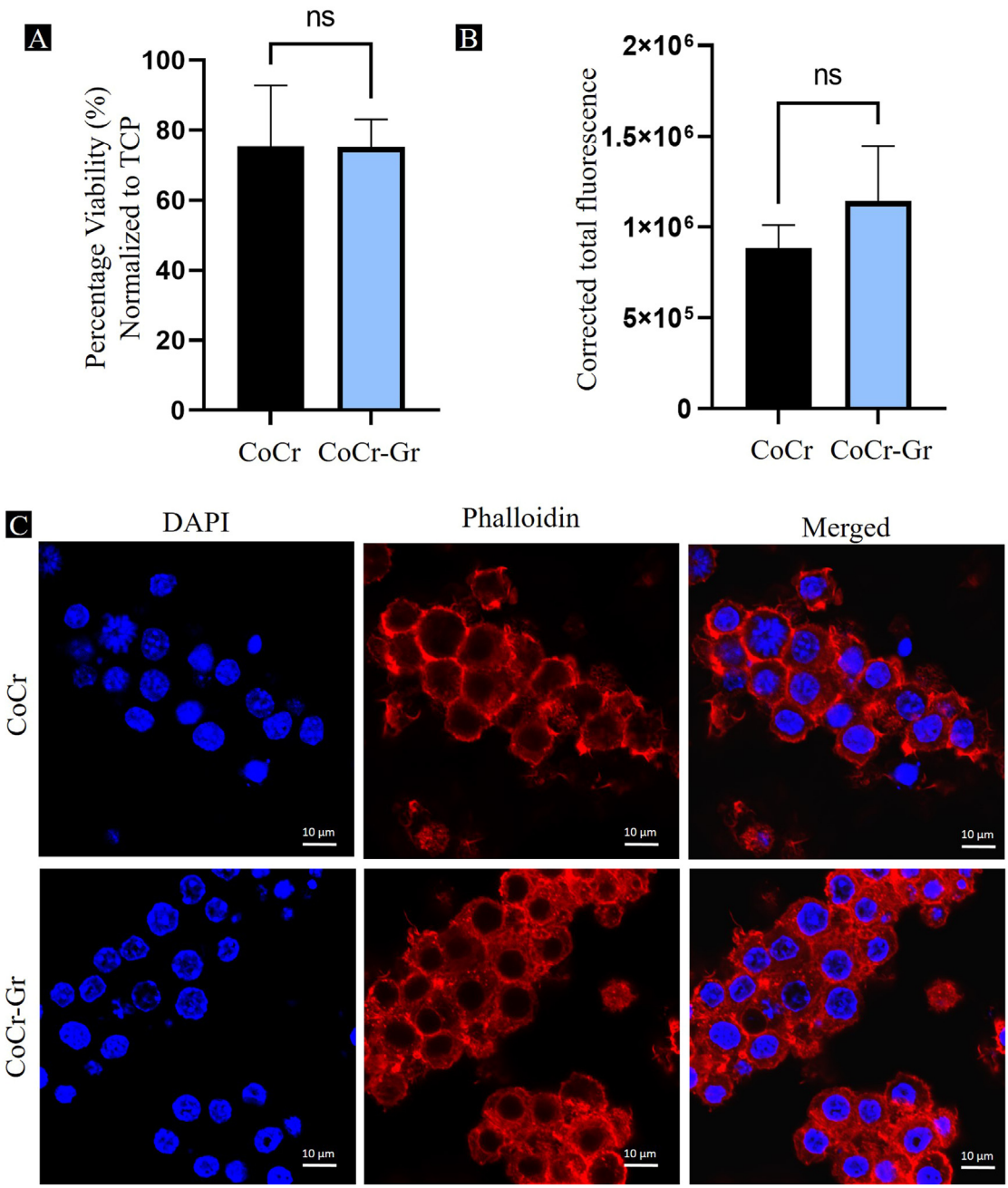

Fig. 3. A shows the MTT assay plot representing the cell viability of RAW macrophages CoCr and CoCr-Gr. Mean ± SD, n = 6 and B display cell fluorescence intensity. C shows morphology and focal adhesion of RAW macrophages after 48 h incubation. The scale bars represent 10 µm.

adherent bacteria were stained with the well-established live/dead assay. After staining live and dead cells are represented by green and red fluorescence, respectively (Fig. 4 A). The bactericidal effect of CoCr-Gr was statistically significant ($p<0.0001$) against *P. aeruginosa* and *S. aureus* ($p<0.01$) when compared to CoCr control surfaces. The antifouling effect was evaluated by quantifying the attachment of bacteria onto both samples. The attachment of *P. aeruginosa* on CoCr-Gr was statistically significantly lower ($p<0.0001$) than on CoCr control surfaces but there were no significant differences in *S. aureus* attachment (Fig. 4 B).

The morphology of *S. aureus* and *P. aeruginosa* incubated in CoCr and CoCr-Gr imaged by SEM is presented in Fig. 5. The CoCr control samples showed healthy bacterial morphology, S. aureus appeared unaffected (A-C), whereas *P. aeruginosa* showed evidence of extracellular polymeric substances (EPS) formation, suggesting the early stage of biofilm formation [41]. In contrast, *S. aureus* and *P. aeruginosa* inoculated on the CoCr-Gr had disrupted and wrinkled cell walls, heavily affected by the Gr coating (Fig. 5 B and 5 D).

S. aureus incubated with CoCr-Gr showed a well-defined EPS connecting bacteria. One of the multiple roles of the EPS matrix is to protect bacteria against mechanical challenges. According to Tu et al. [42], sharp graphene nanosheets can extract phospholipids from bacterial Gram-negative cell membrane by hydrophobic interactions between Gr and the lipid tail of the phospholipid. Another theory from Luan et al. [43] describes that the curvature of the graphene had a significant influence on the lipid extraction process, while Wu et al. [44] identified lipid extraction could be associated with the GO and hydrophilic head

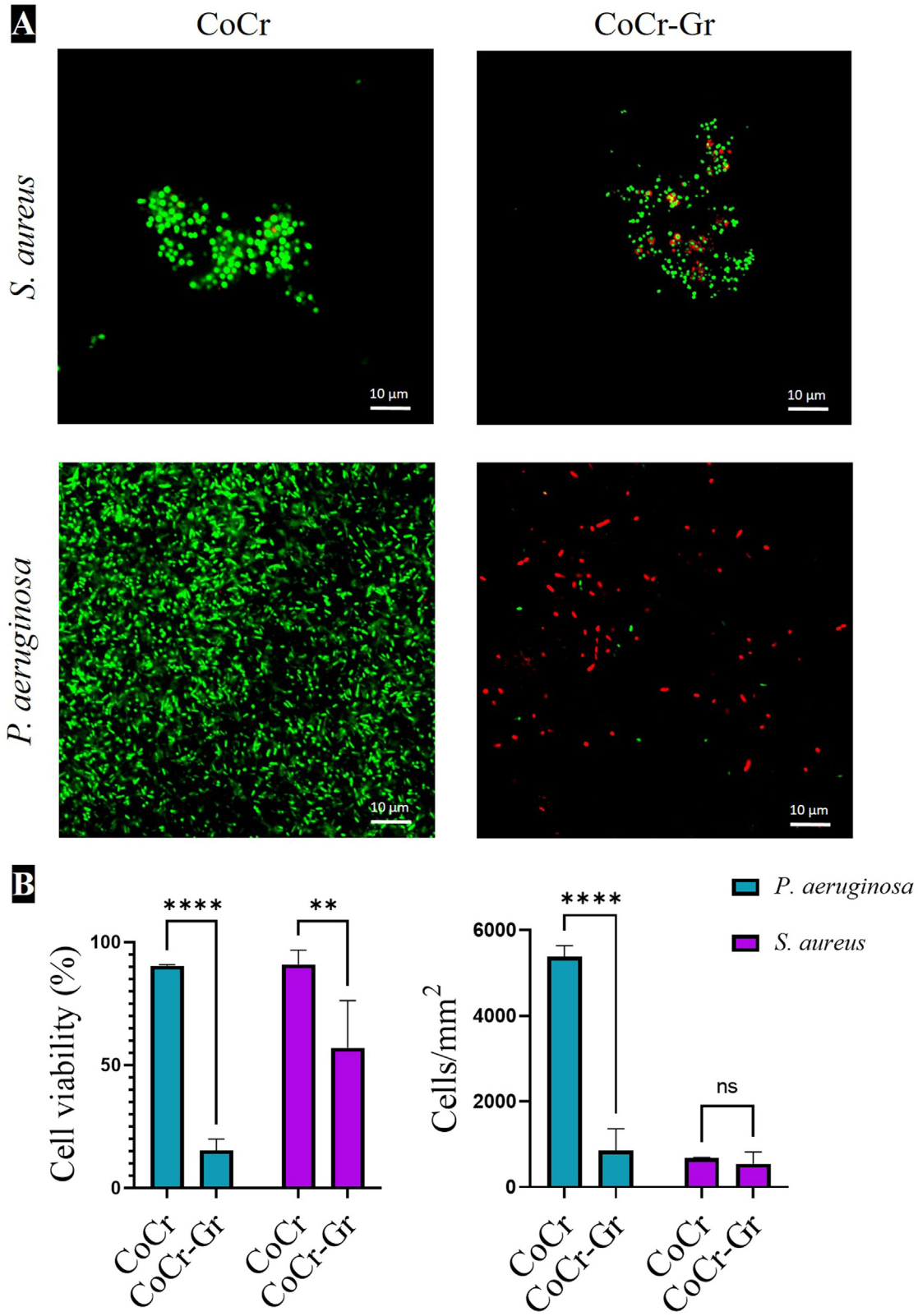

Fig. 4. Fluorescence microscopy images after using LIVE/DEAD staining of *S. aureus* and *P. aeruginosa* and on CoCr and CoCr-Gr are shown in 4 A. Bacterial cell viability percentage and cells per image quantification are represented in 4 B The scale bar represents 10 μm. Bar graphs are presented as mean ± SD, n = 3 ** $p<0.01$ and **** $p<0.0001$.

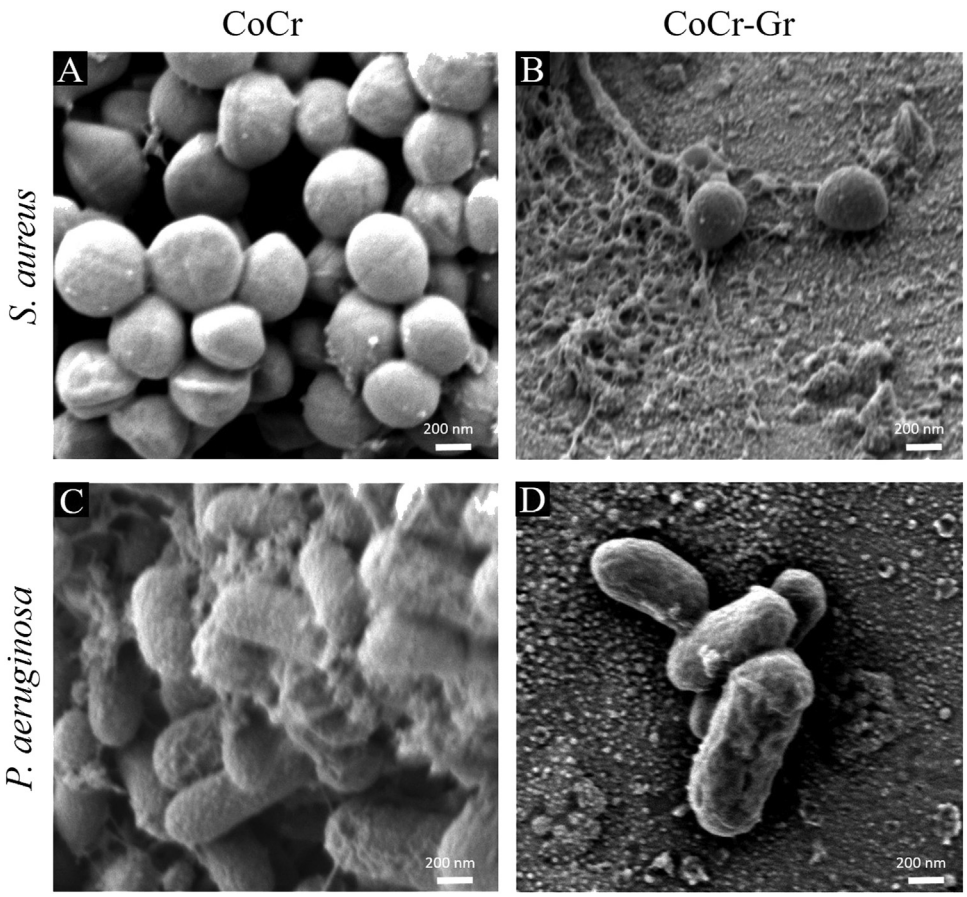

Fig. 5. SEM images of the bactericidal and antifouling effect of CoCr and CoCr-Gr surfaces against *P. aeruginosa* and *S. aureus*. The scale bars indicate 200 nm.

groups of lipids. However, the disruption of the Gram-negative bacterial cell wall by CoCr-Gr could be associated with the shape of the Gr, as well as potential local hydrophobic nano interactions between Gr and phospholipids.

4. Conclusions

Gr was deposited on CoCr substrates using RF-PECVD and *Origanum vulgare* as a Gr precursor. Raman spectroscopy and X-ray photoelectron spectroscopy confirmed the presence of Gr in the CoCr-Gr sample which was multilayered and had a high content of defects. The plasma deposition of Gr on CoCr surfaces did not affect the hydrophilicity of the samples. The SEM microscopies showed Gr in the form of nanostructures with various nanometric shapes and sizes. The biocompatibility results demonstrated that both CoCr and CoCr-Gr had similar viability, adhesion, and morphology of RAW macrophages after 48 h of incubation. The bactericidal and antifouling effect of CoCr-Gr was significantly higher against *P. aeruginosa* compared to the control. CoCr-Gr was also bactericidal against *S. aureus*.

The rapid fabrication of Gr using RF-PECVD on a variety of substrates and a sustainable volatile source of carbon such as *Origanum vulgare* offers versatility and potential for customization in implant design and production.

Overall, the unique combination of properties exhibited by Gr coatings, including high biocompatibility, and antibacterial and antifouling properties make them a promising material for coating medical implants. However, further research is necessary to fully understand the potential of Gr coatings in the context of implant design, production, and use, and to ensure their safety and efficacy in clinical settings.

Declaration of Competing Interest

The authors declare that they have no known competing financial interests or personal relationships that could have appeared to influence the work reported in this paper.

Data availability

Data will be made available on request.

Acknowledgments

Project funding was provided by Krasimir Vasilev, Mohan Jacob, and Jesus Romo-Rico. KV thanks NHMRC for Fellowship GNT1194466 and ARC for grant DP180101254.

JG is supported by funding from Townsville Hospital and Health Services, Tropical Australian Academic Health centre, Heart Foundation, Medical Research Future Fund and the Queensland Government. JG holds a Senior Clinical Research Fellowship from the Queensland Government, Australia.

References

[1] Z. Saleem, B. Godman, M.A. Hassali, F.K. Hashmi, F. Azhar, I.U. Rehman, Point prevalence surveys of health-care-associated infections: a systematic review, Pathog. Glob. Health 113 (4) (2019) 191–205.

[2] J. Sahoo, S. Sarkhel, N. Mukherjee, A. Jaiswal, Nanomaterial-based antimicrobial coating for biomedical implants: new age solution for biofilm-associated infections, ACS Omega 7 (50) (2022) 45962–45980.

[3] A. Trampuz, W. Zimmerli, Diagnosis and treatment of infections associated with fracture-fixation devices, Injury 37 (2) (2006) S59–S66.

[4] K.M.D. Merollini, R.W. Crawford, N. Graves, Surgical treatment approaches and reimbursement costs of surgical site infections post hip arthroplasty in Australia: a retrospective analysis, BMC Health Serv. Res. 13 (1) (2013) 91.

[5] R. Bright, A. Hayles, J. Wood, N. Ninan, D. Palms, R.M. Visalakshan, A. Burzava, T. Brown, D. Barker, K. Vasilev, Bio-inspired nanostructured Ti-6Al-4V alloy: the role of two alkaline etchants and the hydrothermal processing duration on antibacterial activity, Nanomaterials 12 (7) (2022) 1140 Basel.

[6] A.F.P. Carreiro, J.A. Delben, S. Guedes, E.J.D. Silveira, M.N. Janal, C.E. Vergani, S. Pushalkar, S. Duarte, Low-temperature plasma on peri-implant–related biofilm and gingival tissue, J. Periodontol. 90 (5) (2019) 507–515 1970.

[7] T.-F.C. Mah, G.A. O'Toole, Mechanisms of biofilm resistance to antimicrobial agents, Trends Microbiol. 9 (1) (2001) 34–39.

[8] A.G. Emelianova, N.V. Petrova, C. Fremez, M. Fontanié, S.A. Tarasov, O.I. Epstein, Therapeutic potential of highly diluted antibodies in antibiotic-resistant infection, Eur. J. Pharm. Sci. 173 (2022) 106161.

[9] A. Hayles, J. Hasan, R. Bright, D. Palms, T. Brown, D. Barker, K. Vasilev, Hydrothermally etched titanium: a review on a promising mechano-bactericidal surface for implant applications, Mater. Today Chem. 22 (2021) 100622.

[10] S. Beyranvand, Z. Pourghobadi, S. Sattari, K. Soleymani, I. Donskyi, M. Gharabaghi, W.E.S. Unger, G. Farjanikish, H. Nayebzadeh, M. Adeli, Boronic acid functionalized graphene platforms for diabetic wound healing, Carbon N Y 158 (2020) 327–336.

[11] M. Shahnawaz Khan, H.N. Abdelhamid, H.F. Wu, Near infrared (NIR) laser mediated surface activation of graphene oxide nanoflakes for efficient antibacterial, antifungal and wound healing treatment, Colloids Surf. B 127 (2015) 281–291.

[12] S. Pandit, Z. Cao, V.R.S.S. Mokkapati, E. Celauro, A. Yurgens, M. Lovmar, F. Westerlund, J. Sun, I. Mijakovic, Vertically aligned graphene coating is bactericidal and prevents the formation of bacterial biofilms, Adv. Mater. Interfaces 5 (7) (2018) 1701331 n/a..

[13] S.Y. Bhong, N. More, M. Choppadandi, G. Kapusetti, Review on carbon nanomaterials as typical candidates for orthopaedic coatings, SN Appl. Sci. 1 (1) (2018) 76.

[14] A. Mazinani, M.J. Nine, R. Chiesa, G. Candiani, P. Tarsini, T.T. Tung, D. Losic, Graphene oxide (GO) decorated on multi-structured porous titania fabricated by plasma electrolytic oxidation (PEO) for enhanced antibacterial performance, Mater. Des. 200 (2021) 109443.

[15] N. Safari, N. Golafshan, M. Kharaziha, M.Reza Toroghinejad, L. Utomo, J. Malda, M. Castilho, Stable and antibacterial magnesium–graphene nanocomposite-based implants for bone repair, ACS Biomater. Sci. Eng. 6 (11) (2020) 6253–6262.

[16] B. Singh, G. Singh, B.S. Sidhu, *In vitro* investigation of NbTa alloy coating deposited on CoCr alloy for biomedical implants, Surf. Coat. Technol. 377 (2019) 124932.

[17] M.C. Garcia-Mendez, V.H. Urrutia-Baca, C.A. Cuao-Moreu, E. Lorenzo-Bonet, M. Alvarez-Vera, D.M. Ortiz-Martinez, M.A. de la Garza-Ramos, *In vitro* biocompatibility evaluation of a new Co-Cr-B alloy with potential biomedical application, Metals 11 (8) (2021) 1267 Basel.

[18] B. Stojanović, C. Bauer, C. Stotter, T. Klestil, S. Nehrer, F. Franek, M.Rodríguez Ripoll, Tribocorrosion of a CoCrMo alloy sliding against articular cartilage and the impact of metal ion release on chondrocytes, Acta Biomater. 94 (2019) 597–609.

[19] K. Shukla, A.A. Sugumaran, I. Khan, A.P. Ehiasarian, P.E. Hovsepian, Low pressure plasma nitrided CoCrMo alloy utilising HIPIMS discharge for biomedical applications, J. Mech. Behav. Biomed. Mater. 111 (2020) 104004.

[20] N.A. Hodges, E.M. Sussman, J.P. Stegemann, Aseptic and septic prosthetic joint loosening: impact of biomaterial wear on immune cell function, inflammation, and infection, Biomaterials 278 (2021) 121127.

[21] A. García-Argumánez, I. Llorente, O. Caballero-Calero, Z. González, R. Menéndez, M.L. Escudero, M.C. García-Alonso, Electrochemical reduction of graphene oxide on biomedical grade CoCr alloy, Appl. Surf. Sci. 465 (2019) 1028–1036.

[22] J. Guo, G. Cao, X. Wang, W. Tang, W. Diwu, M. Yan, M. Yang, L. Bi, Y. Han, Coating CoCrMo alloy with graphene oxide and ε-Poly-L-lysine enhances its antibacterial and antibiofilm properties, Int. J. Nanomed. 16 (2021) 7249–7268.

[23] M.S.A. Kamel, C.T. Stoppiello, M.V. Jacob, Single-step, catalyst-free, and green synthesis of graphene transparent electrode for organic photovoltaics, Carbon N Y 202 (2023) 150–158.

[24] A. Al-Jumaili, M.A. Zafar, K. Bazaka, J. Weerasinghe, M.V. Jacob, Bactericidal vertically aligned graphene networks derived from renewable precursor, Carbon Trends 7 (2022) 100157.

[25] A. Al-Jumaili, P. Mulvey, A. Kumar, K. Prasad, K. Bazaka, J. Warner, M.V. Jacob, Eco-friendly nanocomposites derived from geranium oil and zinc oxide in one step approach, Sci. Rep. 9 (1) (2019) 5973.

[26] Z. Sheikh, P.J. Brooks, O. Barzilay, N. Fine, M. Glogauer, Macrophages, foreign body giant cells and their response to implantable biomaterials, Materials 8 (9) (2015) 5671–5701 Basel.

[27] M.Y. Svavil'nyi, V.Y. Panarin, A.A. Shkola, A.S. Nikolenko, V.V. Strelchuk, Plasma enhanced chemical vapor deposition synthesis of graphene-like structures from plasma state of CO2 gas, Carbon N Y 167 (2020) 132–139.

[28] Z.Muhammad Adeel, L. Yang, A. Scarlett, V.J. Mohan, Electrochemical sensing of oxalic acid using silver nanoparticles loaded nitrogen-doped graphene oxide, Carbon Trends 8 (2022) 100188.

[29] M.A. Zafar, M.V. Jacob, Synthesis of free-standing graphene in atmospheric pressure microwave plasma for the oil-water separation application, Appl. Surf. Sci. Adv. 11 (2022) 100312.

[30] K.Y. Law, Definitions for hydrophilicity, hydrophobicity, and superhydrophobicity: getting the basics right, J. Phys. Chem. Lett. 5 (4) (2014) 686–688.

[31] M. Ramiasa-MacGregor, A. Mierczynska, R. Sedev, K. Vasilev, Tuning and predicting the wetting of nanoengineered material surface, Nanoscale 8 (8) (2016) 4635–4642.

[32] L. Lv, Y. Xie, K. Li, T. Hu, X. Lu, Y. Cao, X. Zheng, Unveiling the mechanism of surface hydrophilicity-modulated macrophage polarization, Adv. Healthc. Mater. 7 (19) (2018) e1800675-n/a.

[33] R.M. Visalakshan, M.N. MacGregor, S. Sasidharan, A. Ghazaryan, A.M. Mierczynska-Vasilev, S. Morsbach, V. Mailänder, K. Landfester, J.D. Hayball, K. Vasilev, Biomaterial surface hydrophobicity-mediated serum protein adsorption and immune responses, ACS Appl. Mater. Interfaces 11 (31) (2019) 27615–27623.

[34] C.G. Sokolik, J.P. Lellouche, Hybrid-silica nanoparticles as a delivery system of the natural biocide carvacrol, RSC Adv. 8 (64) (2018) 36712–36721.

[35] Database, XPS (X-ray Photoelectron Spectroscopy), XPS Spectra – Chemical Shift|Binding Energy http://techdb.podzone.net/xpsstate-e/(2015).

[36] J. Romo-Rico, S. Murali Krishna, J. Golledge, A. Hayles, K. Vasilev, M.V. Jacob, Plasma polymers from oregano secondary metabolites: antibacterial and biocompatible plant-based polymers, Plasma Process. Polym. 19(7) (2022) n/a.

[37] J.H. María, M. Denise, B. Igor, N. Victor, O.I. Gonzalo, Chemical changes of graphene oxide thin films induced by thermal treatment under vacuum conditions, Coatings 10 (2) (2020) 113 Basel.

[38] J. Augustyn-Pieniazek, A. Lukaszczyk, R. Zapala, Microstructure and corrosion resistance characteristics of Cr-Co-Mo alloys designed for prosthetic materials, Arch. Metall. Mater. 58 (4) (2013) 1281.

[39] M.V. Jacob, R.S. Rawat, B. Ouyang, K. Bazaka, D.S. Kumar, D. Taguchi, M. Iwamoto, R. Neupane, O.K. Varghese, Catalyst-Free Plasma Enhanced Growth of Graphene from Sustainable Sources, Nano Lett. 15 (9) (2015) 5702–5708.

[40] Y.L. Fan, H.C. Zhao, B. Li, Z.L. Zhao, X.Q. Feng, Mechanical roles of F-actin in the differentiation of stem cells: a review, ACS Biomater. Sci. Eng. 5 (8) (2019) 3788–3801.

[41] L. Kirchhoff, D. Arweiler-Harbeck, J. Arnolds, T. Hussain, S. Hansen, R. Bertram, J. Buer, S. Lang, J. Steinmann, B. Höing, Imaging studies of bacterial biofilms on cochlear implants-Bioactive glass (BAG) inhibits mature biofilm, PLOS One 15 (2) (2020) e0229198.

[42] Y. Tu, M. Lv, P. Xiu, T. Huynh, M. Zhang, M. Castelli, Z. Liu, Q. Huang, C. Fan, H. Fang, R. Zhou, Destructive extraction of phospholipids from Escherichia coli membranes by graphene nanosheets, Nat. Nanotechnol. 8 (8) (2013) 594–601.

[43] B. Luan, T. Huynh, R. Zhou, Complete wetting of graphene by biological lipids, Nanoscale 8 (10) (2016) 5750–5754.

[44] L. Wu, L. Zeng, X. Jiang, Revealing the nature of interaction between graphene oxide and lipid membrane by surface-enhanced infrared absorption spectroscopy, J. Am. Chem. Soc. 137 (32) (2015) 10052–10055.